

Fabrication of an ideal nanoring from a black phosphorus nanoribbon upon movable bundling carbon nanotubes

This content has been downloaded from IOPscience. Please scroll down to see the full text.

2017 Nanotechnology 28 385603

(<http://iopscience.iop.org/0957-4484/28/38/385603>)

View [the table of contents for this issue](#), or go to the [journal homepage](#) for more

Download details:

IP Address: 150.203.213.33

This content was downloaded on 02/09/2017 at 02:19

Please note that [terms and conditions apply](#).



NANORAMAN: Multi Technique Analysis
Platform from **MACRO** to **NANOSCALE**

[Learn more >>](#)

HORIBA
Scientific

Fabrication of an ideal nanoring from a black phosphorus nanoribbon upon movable bundling carbon nanotubes

Kun Cai^{1,2}, Jiao Shi¹, Lingnan Liu¹ and Qing H Qin²

¹College of Water Resources and Architectural Engineering, Northwest A&F University, Yangling 712100, People's Republic of China

²Research School of Engineering, the Australian National University, ACT, 2601, Australia

E-mail: Qinghua.qin@anu.edu.au

Received 15 June 2017, revised 9 July 2017

Accepted for publication 17 July 2017

Published 1 September 2017



CrossMark

Abstract

As a low dimensional material, black phosphorus (BP) continues to attract much attention from researchers due to its excellent electric properties. In particular, the one-dimensional material, in the form of a ring or tube formed from BP, has been extensively studied and found to be a perfect semiconductor. But the BP ring has never been reported in laboratories. To form an ideal ring from a rectangular BP ribbon, we choose a carbon nanotube (CNT) bundle to attract the ribbon and move one or more CNTs in the bundle to induce the unsaturated ends of the BP ribbon to become covalently bonded. Numerical experiments are applied to BP ribbons with lengths either equal to, shorter, or longer than the perimeter of the CNT bundle, to investigate the formation of a BP ring. Experiments show that if one end of the BP ribbon is attracted by a CNT, moving the other CNTs away endows the ribbon with high probability of forming an ideal ring. The conclusions drawn from these results will benefit future *in situ* experiments involving forming a ring from a BP ribbon.

Supplementary material for this article is available [online](#)

Keywords: black phosphorus, nanoribbon, nanoring, nanotube, molecular dynamics

(Some figures may appear in colour only in the online journal)

1. Introduction

Phosphorus has many allotropes, among which black phosphorus (BP) behaves as an important van der Waals (vdW) semiconductor. Studies have shown that few-layered BP has a finite and direct band gap [1], high free carrier mobility at room temperature [2], and anisotropic electric conductance [3]. Due to its excellent electric properties, BP has wide potential applications in transistors, logic, and optoelectronic devices.

Lower dimensional materials with special quantum mechanics properties are essential in nano-electro-mechanical systems. It is well known that carbon also has many allotropes with different dimensional configurations, e.g., fullerene in 0D [4], the carbon nanotube (CNT) in 1D [5, 6], graphene in 2D [7], and diamond in 3D. Sometimes a CNT can be

considered as a nanostructure fabricated from a tailored graphene along a specific direction [8, 9]. Both multi-layered graphene and multi-walled CNTs have two merits: strong in-plane/shell bonds and weak inter-layer/shell interaction [10–12]. These properties are attributed to the layout of covalent electrons (i.e., $2sp^2$) in a carbon atom. Correspondingly, each phosphorus atom in BP is covalently bonded ($3sp^3$) with three neighboring atoms. Hence, both the stiffness and the strength of BP [13, 14] are far lower than those of graphene. This layout of the covalent electrons also makes the electric properties of BP outstanding.

It is important for a component in a nanodevice to be stable in extreme working conditions. However, experiments have shown that BP is unstable in air or water environments [15–19]. When exposed to air, the phosphorus atoms in BP react quickly with O_2 and/or H_2O . The BP-based component

therefore fails due to degradation of the BP. To bypass this problem, many surface passivation techniques have been proposed to protect BP from corrosion [16, 20–22]. Yet the duration of protection of BP needs to be enhanced when it is used in nanodevices. Since the end atoms of BP show higher chemical activity than the inner atoms, reducing the number of end atoms in BP can be a feasible way to improve the duration of its protection. One approach to reducing the number of end atoms is to covalently bond two ends of BP to form a nanotube or nanoring (larger perimeter) from a BP nanoribbon, but the layout of covalent bonds makes it difficult for BP to form a shelled 1D material, e.g., a nanotube or nanoring, by chemosynthesis method. To the authors' knowledge, there is no report of BP rings even in a laboratory, although BP nanotubes have attracted much attention recently [23–26]. It should also be mentioned that the nanoring has a wide application in practical engineering applications such as photodetectors [27], waveguide pairs [28], biosensors [29], energy harvesting [30], and catalysis [31]. Hence, exploration of 1D phosphorus material fabrication from a BP ribbon is worthwhile.

There are several well-documented methods for the fabrication of nanorings. Lu *et al* [32] synthesized a hexabenzocoronene-containing cycloparaphenylene carbon nanoring using metal-mediated cross-coupling reactions. Halpern *et al* [33] presented a nanoring array fabrication method by combining the process of lithographically patterned nanoscale electrodeposition with colloidal lithography. Hobbs *et al* [34] fabricated ordered arrays of Au, Ni, and Si nanorings using Ar⁺ sputter redeposition of material in a porous alumina mask. Cui *et al* [35] presented a method for fabricating metal nanoring arrays by means of nanoimprint lithography, physical vapor deposition, and dry and wet etching. Chien and Wu [36] reported a method for fabricating size-tunable hierarchical porous Cr nanoring arrays using modified nanosphere lithography-based technology. However, these existing methods seem unsuitable or inefficient for fabricating BP nanotubes or rings. That is the motivation for developing an efficient method for fabricating ideal BP rings. It is noted from our previous study that a nanotube from a BP ribbon can be fabricated on a CNT by self-assembly [26, 37]. The success of this fabrication is attributed to the following reasons. First, the attraction between the BP ribbon and the CNT is strong enough to bend the BP ribbon along the armchair direction, which is the major power to drive the self-assembling process. Second, bending a BP ribbon along the armchair direction is much easier than along the zigzag direction. The bending leads the ends along the zigzag direction to remain parallel when the ribbon is attracted onto a CNT. Third, the BP ribbon can sustain a large curvature along the armchair direction [24, 38, 39]. Finally, the vdW interaction between non-bonding phosphorus atoms is far greater than that between phosphorus and carbon atoms [40], an observation that implies that the BP nanotube can move away from the capped CNT without damage. However, our results showed that a BP nanotube formed on a CNT needs to satisfy a length constraint, i.e., the length of the ribbon must be ~ 2.1 nm longer than the circumferential perimeter of the CNT. A shorter BP ribbon

Table 1. Parameters of CNTs and BP ribbons involved in simulations (unit: nm).

Item	CNT(13, 13)	BP 1	BP 2	BP 3	BP 4
Length	7.748	12.62	16.996	17.434	23.998
Width/ radius	0.882	2.32	2.32	2.32	2.32
N	\times	29	39	40	55
Atoms	1664C + 52H	870P	1170P	1200P	1650P

attracted by a CNT cannot form a closed tube. If it is longer, the BP ribbon will become a nanoscroll when wound upon the CNT. In an *in situ* experiment, it is difficult to prepare a BP ribbon with a length that accurately matches a given CNT, or vice versa. In this study, we present a new approach for fabricating a nanoring from a rectangular BP ribbon on a movable CNT bundle. With this method, the preparation of the BP ribbon is independent of the length of the ribbon.

2. Models and methodology

2.1. Models

When the initial configuration of the system is chosen as shown in figure 1, the perfect length of the BP ribbon can be defined. A BP ribbon of the so-called perfect length means that the ribbon can cover one circuit of the CNTs. On the other hand, the length of the BP ribbon should be an integral multiple of L_0 . Hence, the definition of perfect length reads

$$L_p = N \times L_0 = \sim \pi(r_{\text{CNT}} + \sigma_{\text{C-P}} + 0.5d_{\text{BP}}) + 4(n - 1)[2r_{\text{CNT}} + \sigma_{\text{C-C}}], \quad (1)$$

where r_{CNT} is the radius of the CNTs, n is the number of CNTs in the bundle. In the present study, $n = 2$ or 3. $\sigma_{\text{C-P}}$ and $\sigma_{\text{C-C}}$ are the equilibrium distances between CNT and BP/CNT, respectively. Their values can be found in table 2. As the radius of CNT can be larger or more CNTs can be involved, the number of N might not be unique. For example, for a 3-a-type model, the length of the BP ribbon with $N = 39$ or 40 can be considered a perfect length. Clearly, a BP ribbon with a shorter length than the perfect length cannot entirely cover the CNTs, whereas a longer ribbon contains a portion of self-overlap after it covers the CNTs. The length of BP ribbon influences the motion scheme of the CNTs during the formation of a BP ring from the ribbon.

2.2. Methodology

A molecular dynamics (MD) approach is used for obtaining the response of the composite systems investigated. The MD simulations are fulfilled by way of the open source code LAMMPS [41]. In each simulation, interactions among atoms are estimated through the use of empirical potentials. For instance, the interaction between carbon and/or hydrogen atoms

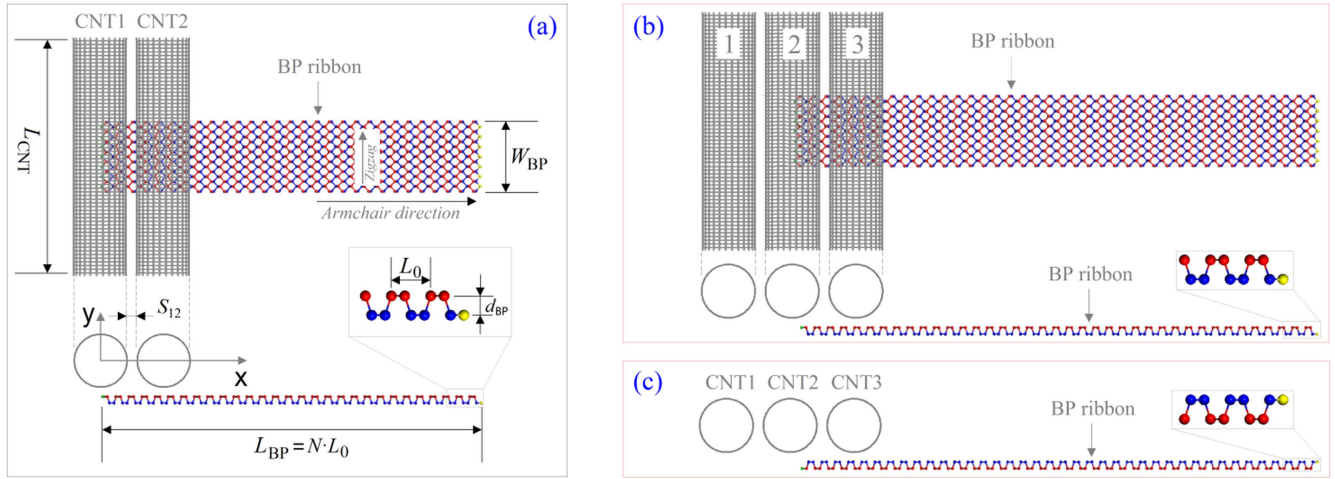


Figure 1. Schematic of geometric model of a system containing one black phosphorus (BP) nanoribbon and a CNT bundle. The parallel carbon nanotubes (CNT) in the bundle are hydrogenated at the ends. L_{BP} and W_{BP} are the length and width of the BP ribbon, respectively. $W_{BP} = \sim 2.32$ nm. $L_0 = \sim 0.44$ nm, which is the unit length of the ribbon along the armchair direction. For forming an ideal BP nanotube, N is an integer. All the tubes have the same chirality and the same length of $L_{CNT} = \sim 7.748$ nm (without considering C–H bonds). The initial value of the surface distance between two neighboring CNTs, labeled S_{12} or S_{23} , is ~ 0.34 nm (equilibrium distance). (a) Two CNTs with an a-type layout BP ribbon, a 2-a-type model, in which the P atoms at the left edge of ribbon is closer to CNT; (b) a 3-a-type model, in which the P atoms at the left edge of BP ribbon is not closer to CNT; (c) a 3-b-type model. In this study, CNTs (13, 13) are used.

Table 2. Parameters in the 12-6 Lennard–Jones potential function among C, H, and P atoms.

Atom i	Atom j	$\sigma_{ij}(\text{nm})$	$\varepsilon_{ij}(\text{eV})$
P	C	0.342 25	0.006 878
P	P	0.3438	0.015 940
C	C	0.3400	0.002 844
C	H	0.3025	0.002 065
H	H	0.2650	0.001 499

in a CNT is estimated by the AIREBO potential [42]. The bonding action among neighbor phosphorus atoms is considered using the Stillinger–Weber potential [43] with the parameters presented by Jiang [44]. The non-bonding interaction among phosphorus and phosphorus/carbon atoms is described by the 12-6 Lennard–Jones potential [45], i.e., between atom i and atom j , the potential can be expressed as

$$\Pi_{ij}^{LJ} = 4\varepsilon_{ij}[(\sigma_{ij}/r_{ij})^{12} - (\sigma_{ij}/r_{ij})^6], \quad (2)$$

where r_{ij} is the spatial distance between atom i and atom j . Other parameters of carbon, hydrogen, and phosphorus atoms are listed in table 2.

The flowchart of a simulation contains the following steps:

Step 1: build CNTs and BP ribbons. Arrange CNTs parallel and locate the left end of a BP ribbon under the right bottom of CNT1 (in 2-a-type model) or CNT2 (in 3-a/b-type model) for a distance of less than 1 nm. Commonly, the distance is about 0.34 nm;

Step 2: fix the ends of the CNTs and the right end of the BP ribbon. Put the system under the canonical NVT ensemble with $T = 8$ K for 1000 ps;

Step 3: after relaxation, release the right end of the BP ribbon;

Step 4: when the system is in a stable state, begin to move one or more CNTs in the system to the specified location along the x -direction. During that period, the configuration of the BP ribbon/scroll changes correspondingly;

Step 5: stop moving CNTs and begin postprocessing.

In the simulation, the time step for the integral of Newton's second law of motion is set to be 0.001 ps.

2.3. Potential energy of the system

It is known that a BP ribbon can be wound easily along the armchair direction [24–26]. The parameters shown in table 2 also indicate that the attraction between carbon and phosphorus atoms is stronger than that between two carbon atoms. Hence, when we release the right end of BP, it will be attracted and quickly wound upon the CNT bundle. During the same period, the surface energy of the system drops quickly. In general, it is difficult for the BP ribbon being wound onto the CNT to form an ideal ring, i.e., the two ends of the BP ribbon are covalently bonded, leading to a sharp drop in potential energy of the ribbon (or system). In that case, a possible strategy that can be adopted is to move one or more CNTs in the bundle to produce other opportunities for forming an ideal BP ring. The current CNTs are arranged in a balanced state. Hence, moving a CNT must lead to an increase in the potential energy of the system. Besides, the motion also leads to further deformation of the BP ribbon, which implies that the potential energy of the ribbon changes simultaneously. Therefore, if we follow the tracks of the variation of potential energy of the system or its components, the variation of the configuration of the system can be adjusted accordingly. Considering this reason, we choose four typical phenomena that can lead to obvious variations in the potential energy of the system.

(a) *Attraction between the BP ribbon and CNT bundle*

In this case, the potential energy of the system varies for two major reasons. One reason is the interaction energy between the ribbon and the bundle:

$$\begin{aligned}\Pi_{P-C} &= \sum_{i=1}^{3N_c} \sum_{j=1}^{N_p} P_{ij}^{LJ} \\ &= \sum_{i=1}^{3N_c} \sum_{j=1}^{N_p} (4\varepsilon_{C-P}[(\sigma_{C-P}/r_{ij})^{12} - (\sigma_{C-P}/r_{ij})^6]),\end{aligned}\quad (3)$$

where N_c is the total number of carbon atoms on each CNT, and N_p is the total number of phosphorus atoms. Considering the cutoff being equal to 1.02 nm in simulation, most phosphorus atoms have an influence on the value of Π_{P-C} at the initial stage. During winding of the BP ribbon onto the CNT bundle, the value of Π_{P-C} varies dramatically, i.e., the distances between phosphorus atoms and carbon atoms decrease quickly.

The second reason is the deformation of the BP ribbon from the initial straight ribbon to the current curved one. The deformation-induced potential energy can be calculated using the equation:

$$\Pi_{\text{Deform}}^{\text{BP}} = \int_0^{L_{\text{BP}}} \frac{W_{\text{Bend}}}{2[\rho(s)]^2} ds + \int_0^{L_{\text{BP}}} \frac{W_{\text{Tens}}}{2} \varepsilon_{\text{Tens}}^2 ds,\quad (4)$$

where W_{Bend} and W_{Tens} are the bending stiffness and tensile stiffness, respectively, of the ribbon when curving along the armchair direction. ρ is the radius of the local curvature of the homogenized BP ribbon, which is approximately equal to $(r_{\text{CNT}} + \sigma_{C-P} + 0.5d_{\text{BP}})$ when it attaches tightly onto a CNT. $\varepsilon_{\text{Tens}}$ is the local tensile strain of the BP ribbon along the armchair direction. Only when the ribbon is pulled by a moving CNT at high speed does the second item in equation (4) become obvious.

(b) *Self-overlap of the BP ribbon*

When the length of the BP ribbon is greater than the perfect length, a certain area near one end of the ribbon must be covered (overlap) by an area near the other end of the ribbon. From table 2, the surface distance between two attached ribbons is ~ 0.3438 nm. Hence, the two parts within the overlap area must have the following interaction energy:

$$\begin{aligned}\Pi_{P-P} &= \sum_{i=1}^{M_p} \sum_{j=1}^{M_p} P_{ij}^{LJ} \\ &= \sum_{i=1}^{M_p} \sum_{j=1}^{M_p} (4\varepsilon_{P-P}[(\sigma_{P-P}/r_{ij})^{12} - (\sigma_{P-P}/r_{ij})^6]),\end{aligned}\quad (5)$$

where M_p is the number of phosphorus atoms within the cutoff neighborhood of the overlap length of the BP

ribbon. Clearly, a longer self-overlap of the ribbon has a higher value of M_p , leading to a lower value of Π_{P-P} .

(c) *Generation or breakage of P-P bonds*

As the C-C bond is far stronger than the P-P bond, perfect CNTs will remain undamaged during moving or being wound by the BP ribbon. Besides, the ends of the CNTs are hydrogenated, i.e., all carbon atoms are saturated. Hence, no C-P covalent bond is being generated. When the CNTs are entwined by the BP ribbon, moving a CNT at high speed may lead to breakage of the ribbon. Data reported in [46] indicated that each new P-P bond being generated will lead to a loss of ~ 0.66 eV of potential energy. In this case, the change in the number of P-P bonds in the ribbon determines the increment of the potential energy of the ribbon, i.e.,

$$\Pi_{\text{React}} = \sim -0.66 \times N_{\text{nb}},\quad (6)$$

where N_{nb} can be considered the variation of the number of P-P bonds in the BP ribbon. When the ribbon is broken, N_{nb} is negative. If an ideal ring is formed from the ribbon, N_{nb} is positive, e.g., 7 in the present study. Otherwise, $N_{\text{nb}} = 0$.

(d) *Moving a CNT away from the bundle*

With the CNTs as shown in figure 1, the interaction energy among them can be expressed as

$$\begin{aligned}\Pi_{C-C} &= (n-1) \sum_{i=1}^{N_c} \sum_{j=1}^{N_c} (4\varepsilon_{C-C}[(\sigma_{C-C}/r_{ij})^{12} - (\sigma_{C-C}/r_{ij})^6]) \\ &\quad + \sum_{k=1}^n \Pi_{\text{Deform}}^{\text{CNT}}.\end{aligned}\quad (7)$$

Hence, moving one CNT away from the CNT bundle will result in an increase in Π_{C-C} . When the distance between the moving CNT and the bundle is longer than the cutoff (1.02 nm), the value of the first item of Π_{C-C} becomes zero for $n = 2$ or half of the current value for $n = 3$. The second item of equation (1) represents the potential energy caused by deformation of the CNTs, which is the difference between the current potential energy of the deformed CNTs and the initial ideal CNTs.

Generally, moving a CNT away can also lead to variation of the potential energy in the previous three cases. Hence, all the cases should be considered simultaneously. The variation of the potential energy of the system can be expressed as

$$\Delta\text{PE} = (\Pi_{P-C} + \Pi_{P-P} + \Pi_{C-C} + \Pi_{\text{React}} + \Pi_{\text{Deform}}^{\text{BP}})'_t - \Pi_{\text{Deform}}^{\text{BP}}|_{t_0},\quad (8)$$

which is the difference between the total potential energy of the system at time t and t_0 . Equation (8) is significant for identifying the state of the system, i.e., the lower the ΔPE , the more stable the system.

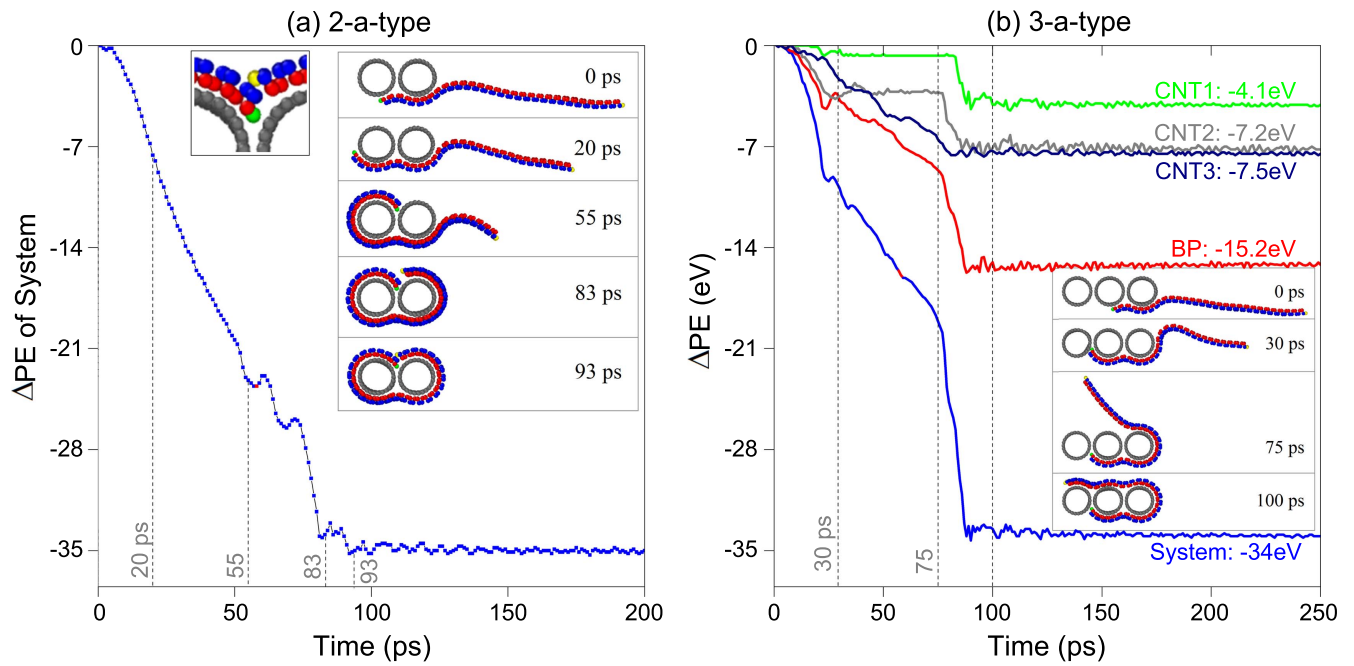


Figure 2. Variation history of potential energy of the system or components with a BP ribbon of $N = 29$. (a) 2-a-type model. (b) 3-a-type model.

3. Numerical tests and discussion

In the following experiments, the initial configuration of a system is obtained by full relaxation of the model shown in figure 1. In relaxation, the boundary conditions have two major aspects. One is that the atoms in the column of phosphorus at the right end of the BP ribbon are fixed. The other is that the atoms within 0.5 nm of the end of each CNT are fixed. When a CNT is moved, the velocities of the atoms previously fixed are set to be identical along the specified direction.

3.1. Possible way to form an ideal BP ring from a short BP ribbon on CNTs

Here we choose a BP ribbon with the perfect length when winding upon a 2-a-type model (movie 1 is available online at stacks.iop.org/NANO/28/385603/mmedia). The history of ΔPE of the system, i.e., the increment of the potential energy of the system, is shown in figure 2(a), together with four typical snapshots. From the configuration of the system at 93 ps, the two ends of the BP ribbon are not covalently bonded (see the upper-left insert in figure 2(a)). The reason is that the end with green atoms is attracted and trapped at the corner between CNT1 and CNT2. Hence, the other end (with yellow atoms) has no opportunity to be covalently bonded with it. The results in figure 2(a) indicate that a BP ribbon with perfect length cannot form an ideal ring without moving any CNT in the CNT bundle entwined by the wound ribbon.

Now, we choose the same BP with $N = 29$ winding upon a 3-a-type model. As shown in figure 2(b), the BP ribbon cannot form an ideal ring here, either. During winding of the ribbon (movie 2), the ΔPE of each component experiences a different drop. For instance, the ΔPE of CNT1 drops 4.1 eV only, far less than that of the BP ribbon (i.e., 15.2 eV). The

reason is that the BP ribbon is attracted to the CNT bundle and only part of CNT1 and the ribbon are attached. CNT2 and CNT3 experience the same drop in potential energy. From the curve of the ΔPE of system, the configuration at 100 ps can be considered as a stable state of the system. This outcome also implies that the winding process needs only ~ 100 ps.

From the snapshot at 100 ps in figure 2(b), we find that the green end of the BP ribbon is also trapped at the corner between CNT1 and CNT2. Now we adopt two approaches to move a CNT in the CNT bundle to determine whether that can induce an ideal ring from the ribbon. First, CNT3 is moved right at a constant speed of 10 m s^{-1} . From the snapshots in figure 3(a), we find that the lower green end of the BP ribbon does not move until the upper yellow end of the ribbon is separated from CNT2 (mid CNT). Hence, the attraction of the corner between CNT1 and CNT2 on the green end is much stronger than that on the other end of the ribbon. When the upper end of the ribbon leaves CNT2, it quickly attaches to the mid part of the ribbon. The attraction between the upper yellow end and the mid part of the ribbon is stronger than that between the green end and CNTs, a phenomenon that can be explained simply, e.g., $\sigma_{P-P} > \sigma_{P-C}$ in table 2. The fluctuation of the ΔPE of the system is actually caused by the swinging of the cantilever part of the BP ribbon (movie 3). This property is significant to the present approach for forming an ideal ring from the BP ribbon. If the attraction between phosphorus and carbon atoms is stronger, CNT3 cannot carry the ribbon away after 93 ps. The ribbon is attracted and attached to CNT1 and CNT2, as shown in figure 2(a).

The second approach is to move CNT1 to the left at a constant speed of 10 m s^{-1} . As shown in figure 3(b), in the initial stage, the lower green end of the BP ribbon at first crosses the gap between CNT1 and CNT2, due to the strong

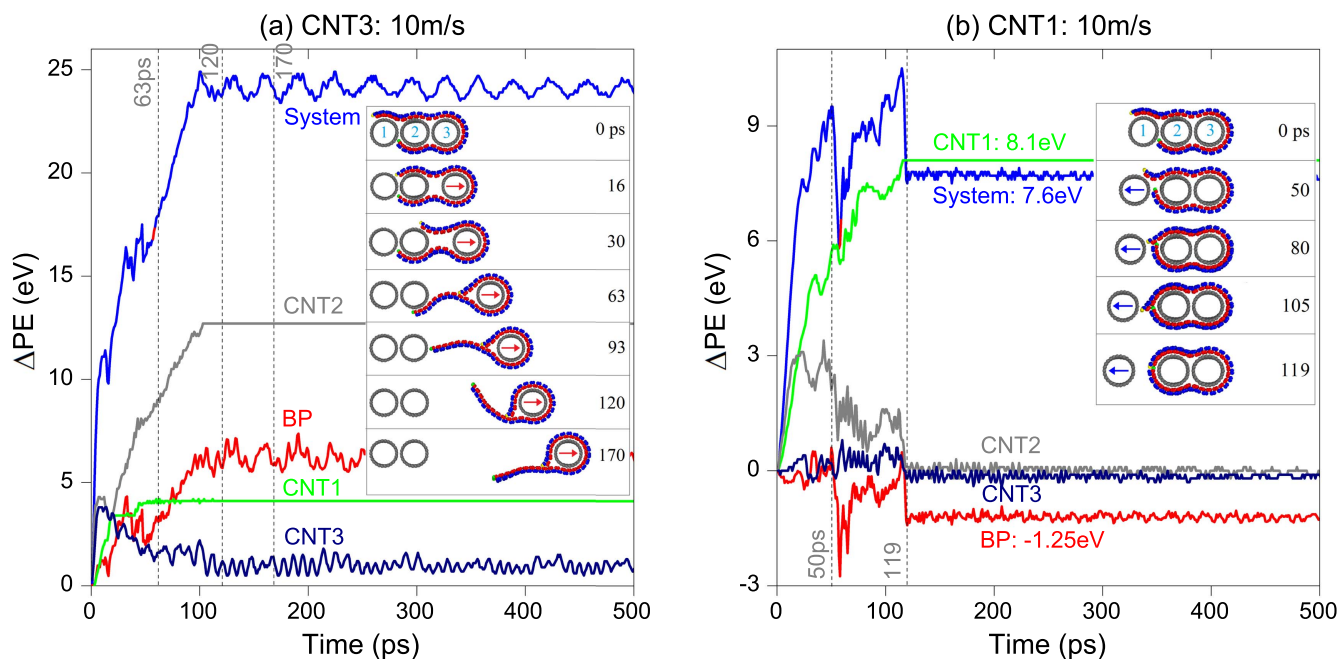


Figure 3. Variation of the potential energy of the system in the 3-a-type model with BP ribbon of $N = 29$. (a) When CNT3 moves to the right (red arrows \rightarrow) at 50 m s^{-1} . (b) When CNT1 moves to the left (blue arrows \leftarrow) at 10 m s^{-1} .

attraction (e.g., the snapshot at 50 ps). In the second stage, the lower green end attaches to the ribbon while the upper end is still attracted to CNT1 (e.g., the snapshot at 105 ps). In the final stage, the two ends of the ribbon are covalently bonded together and an ideal ring is formed when the attraction of CNT1 to the ribbon decreases quickly (movie 4). This variation of the system configuration can also be verified from the curves of ΔPE of components in figure 3(b), e.g., the moving away of CNT1 leads to an increase in the ΔPE of 8.1 eV. The ΔPE of CNT3 tends to be zero because its state experiences very little change. The ΔPE of CNT2 decreases by about 3 eV because of the expansion of the overlap with the BP ribbon/ring. The ΔPE of the BP is $\sim -1.25 \text{ eV}$, indicating that covalent bonds are formed (see the snapshot at 119 ps). The reason is that the local configuration at the joint of the two adjacent ends of the ribbon/ring experiences a small change, implying that there is a slight change in the non-covalent bonding interaction. The sharp drop of potential energy is caused by the formation of covalent bonds between the two ends.

By comparing the final configurations of the system in figures 2(a) and 3(b), we find that an ideal BP ring can be obtained if neither end of the ribbon is trapped at the corner of two neighboring CNTs in the bundle. Hence, the essential step in forming a ring is to drag one of the neighboring CNTs away to allow both ends of the ribbon the opportunity to be united.

Figure 3 shows that the two curves with respect to 'system' and 'BP' fluctuate almost synchronously. This finding indicates that the variation of the ΔPE of the BP ribbon can also be shown by the variation of the ΔPE of the system. Hence, in the following analysis, we present the histories of the ΔPE of the system only. If necessary, both curves are given simultaneously.

3.2. Forming an ideal ring from a BP ribbon with perfect length

From the above discussion, we know that an ideal ring can be formed from a BP ribbon based on two conditions: (1) at least one CNT is able to move away, and (2) no end of the ribbon is trapped in a corner of neighboring CNTs. Hence, in the CNT bundle, the number of tubes should be equal to and greater than 3. Meanwhile, the length of the ribbon in the above numerical experiments is shorter than the perfect length of the BP ribbon in a 3-a/b-type model. If, for example, the length of the BP ribbon is very close to the perfect length, e.g., $N = 39$ or 40 , how can we form an ideal ring from the ribbon?

Before moving a CNT in the 3-tube bundle, we observe the self-winding processes of the ribbon with $N = 39$ in both the 3-a-type and 3-b-type models. Figure 4(a) shows that no BP ring is formed from the ribbon, for the same reason as in the 2-a-type model. If we rotate the ribbon by 180° along the x -direction to change the 3-a-type model into a 3-b-type model (figure 4(b)), the final configuration of the system is a ring, as also verifiable by either the local configuration of the ribbon's joining of its two ends or the sharp drop in the ΔPE value of the system during [145, 155] ps (movie 5). However, this ring is not ideal, as the red phosphorus atoms should be distributed periodically over the whole ring. In the formation of an ideal ring this case should be avoided.

When a BP ribbon with $N = 40$ is used in the experiments, as shown in figure 5(a), the two ends of the BP ribbon overlap at 158 ps, rather than bonding together. Considering the equilibrium distance between the ribbon and CNTs, one CNT is now moved away with a specified displacement to see whether the ribbon can form an ideal ring. For example, by moving CNT1 0.45 nm to left (left insertion in figure 5(b)), the lower green end of the ribbon enters the gap between CNT1 and CNT2, and attaches to the mid part of the ribbon.

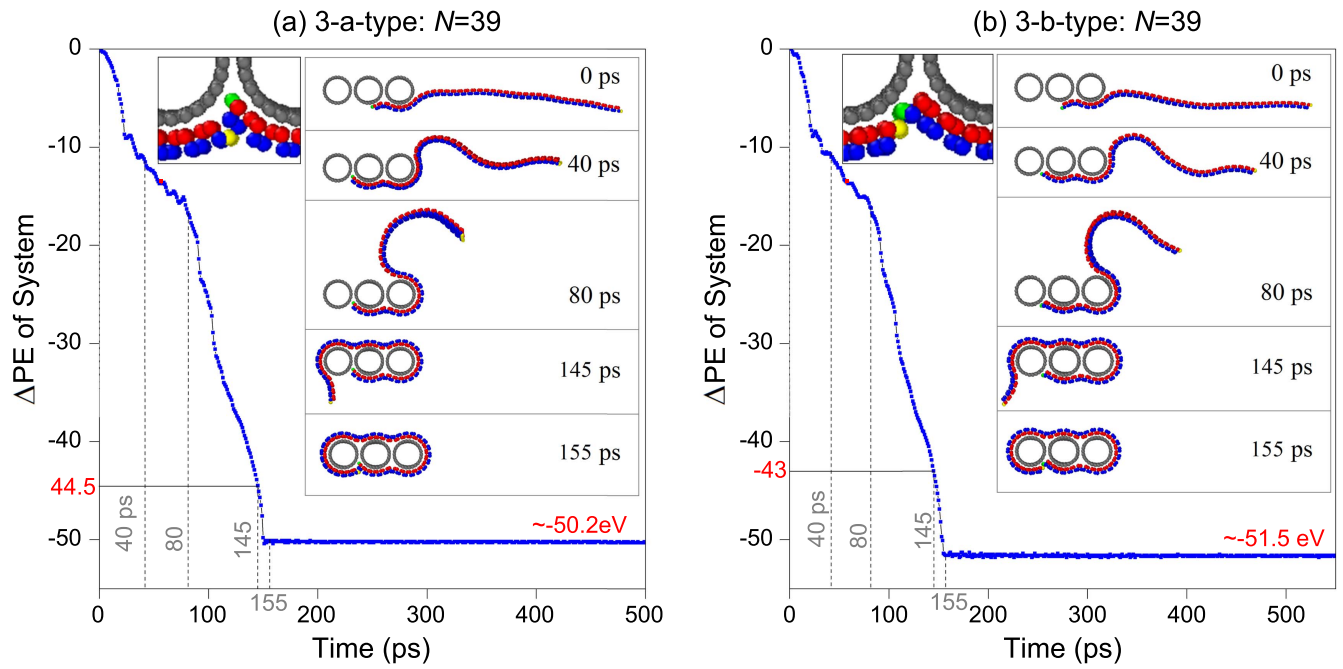


Figure 4. Histories of the variation of potential energy of the system with BP ribbon of $N = 39$. (a) 3-a-type model. (b) 3-b-type model.

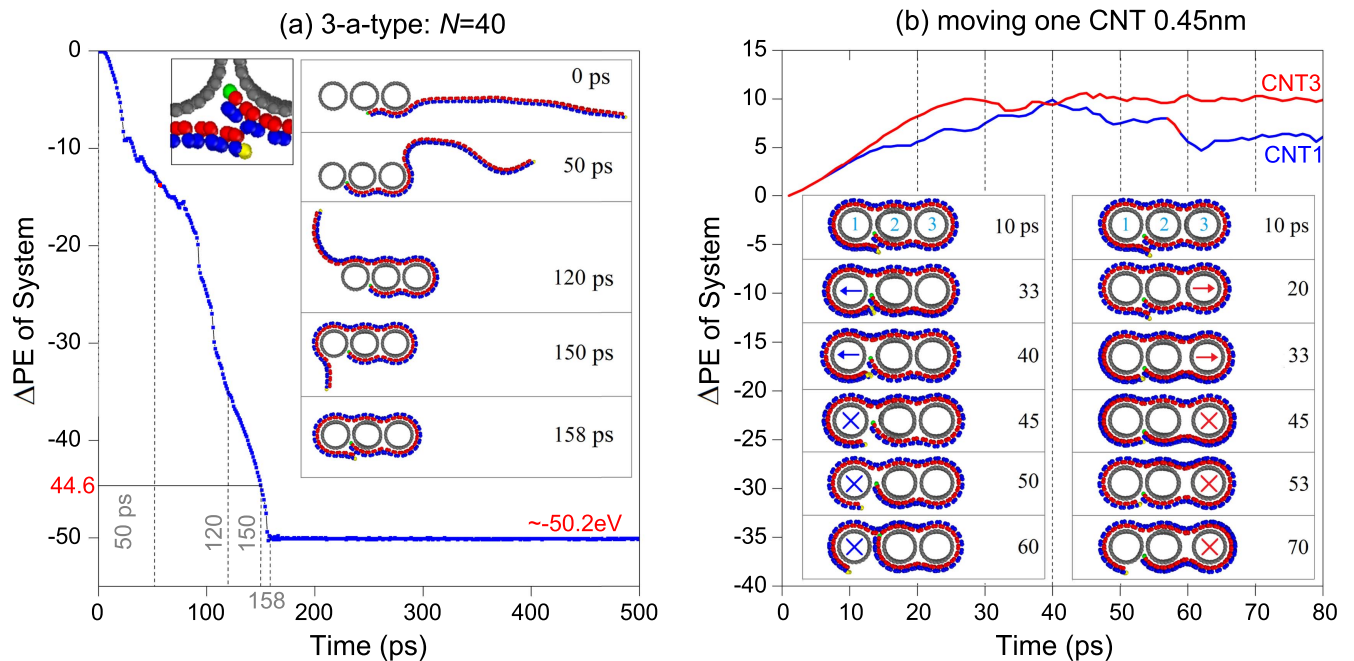


Figure 5. History of the potential energy variation of the 3-a-type system with BP ribbon of $N = 40$. (a) Winding process. (b) CNT1 moves to left (\leftarrow) at 10 m s^{-1} and stops (blue X) after 45 ps; CNT3 moves to right (\rightarrow) at 10 m s^{-1} and stops (red X) after 45 ps.

The situation is similar to that in figure 3(b) at 80 ps. On the other hand, if we move CNT3 0.45 nm to the right (right insertion in figure 5(b)), the final configuration of the system is similar to the initial configuration shown in figure 3(b).

Can the ribbon in figure 5(b) form an ideal ring if we move CNT1 or CNT3 away? To answer this question, we carry out tests with complex movements of CNTs, as shown in figure 6. First, we move CNT1 0.45 nm to the left. Second, we stop the motion of CNT and begin 500 ps of relaxation. The configuration at 545 ps is similar to that at 60 ps shown in

figure 5(b). Third, after relaxation, we move CNT3 by 1.85 nm and stop it at 730 ps. During this period, the lower green end of the ribbon stays still, while the upper yellow end approaches the lower end due to the tension from CNT3. Finally, we begin further motion of CNT1 at a speed of 10 m s^{-1} . As CNT1 moves gradually away, the attraction reduces continuously. Meanwhile, the attraction of CNT2 and CNT3 on the mid part of the ribbon becomes stronger, leading to concavity of the ribbon between CNT2 and CNT3. Fortunately, the upper end does not separate from the lower

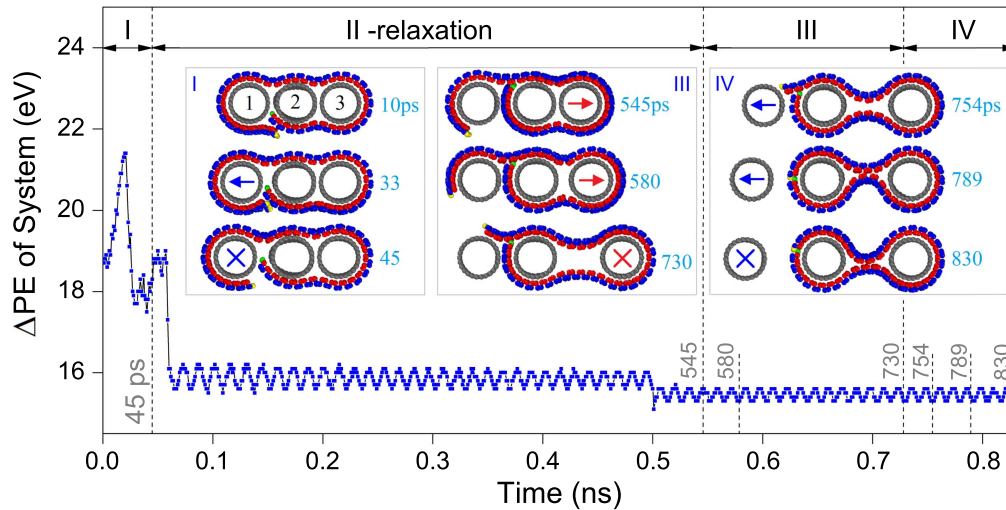


Figure 6. History of the potential energy variation of the 3-a-type system with $N = 40$ at 8 K. It consists of four steps moving the CNTs at the speed of 10 m s^{-1} . In step 1, fix both CNT2 and CNT3, move CNT1 0.45 nm to the left (stops at 45 ps); in step 2, fix all CNTs and relax the system for 500 ps (stops at 545 ps); in step 3, fix both CNT1 and CNT2, move CNT3 1.85 nm to the right (stops at 730 ps); in step 4, fix both CNT2 and CNT3, move CNT1 1.0 nm to the left (stops at 830 ps).

end during this period, and the two ends are bonded together to form an ideal ring (at 789 ps) (movie 6).

In the above process of forming an ideal ring from the BP ribbon, the mid CNT, i.e., CNT2, does not move. The major role of the mid CNT is to attract both ends of the ribbon simultaneously. Attachment of the lower end onto the mid part of the BP ribbon develops due to the strong attraction by the mid CNT. In this situation, further motion of the right CNT, i.e., CNT3, can draw together both ends of the ribbon. From this finding, we conclude that a long BP ribbon can turn into an ideal ring by the following steps. First, use a CNT bundle with larger perimeter to attract the ribbon. Second, locate the mid CNT, which does not move in whole operation. Third, move CNTs at the left or right of the mid CNT to allow one end of the ribbon to attach to the rest of the ribbon. Finally, generate further motion on either left or right CNTs to allow both ends of the ribbon to join.

3.3. Forming an ideal ring from a longer BP ribbon

In the above discussion, the self-overlap of the BP ribbon is very small. Sometimes, in a prepared BP sample, its length may be obviously greater than the perfect length with respect to the CNT bundle involved in the experiment. For example, a BP ribbon with $N = 55$ is placed near a 3-tube bundle as shown in figure 7. Can this ribbon form an ideal ring? Before answering this question, we move only one CNT at different speeds to test whether the BP ribbon breaks. As we know, the speed of moving a probe in transmission electron microscopy is far less than 10 m s^{-1} . The reason for adopting a high speed is to save computational cost. From the results in figure 8, we find that the ribbon does not break when either CNT1 or CNT3 is moved at the speed of 10 m s^{-1} . However, the ribbon breaks if the speed of CNT1 or CNT3 is 50 m s^{-1} . Hence, the speed of 10 m s^{-1} is used in this study to avoid unexpected results.

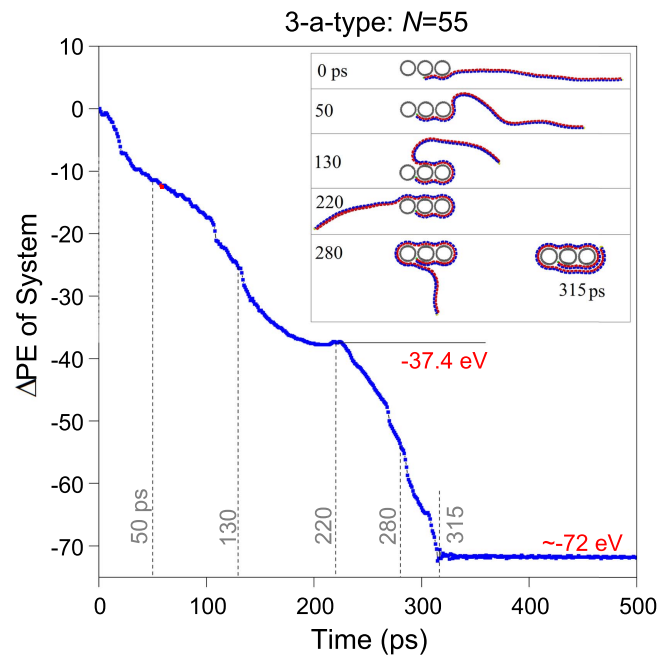


Figure 7. History of the potential energy variation of the a 3-a-type system with BP ribbon of $N = 55$ and 3 CNTs.

(a) Move only one CNT.

(b) Move more than one CNT.

In this numerical experiment of forming a ring from the BP ribbon with $N = 55$, we choose two schemes of motion of CNTs. Before moving the CNTs, the system has stable configuration, i.e., the snapshot at 315 ps in figure 7, is used as the initial state. In each motion, the speed of a CNT is 10 m s^{-1} . The details of the two schemes are as follows:

Scheme 1: (I) fix both CNT1 and CNT2, move CNT3 with a displacement to the right for 5.0 nm, and stop; (II) fix

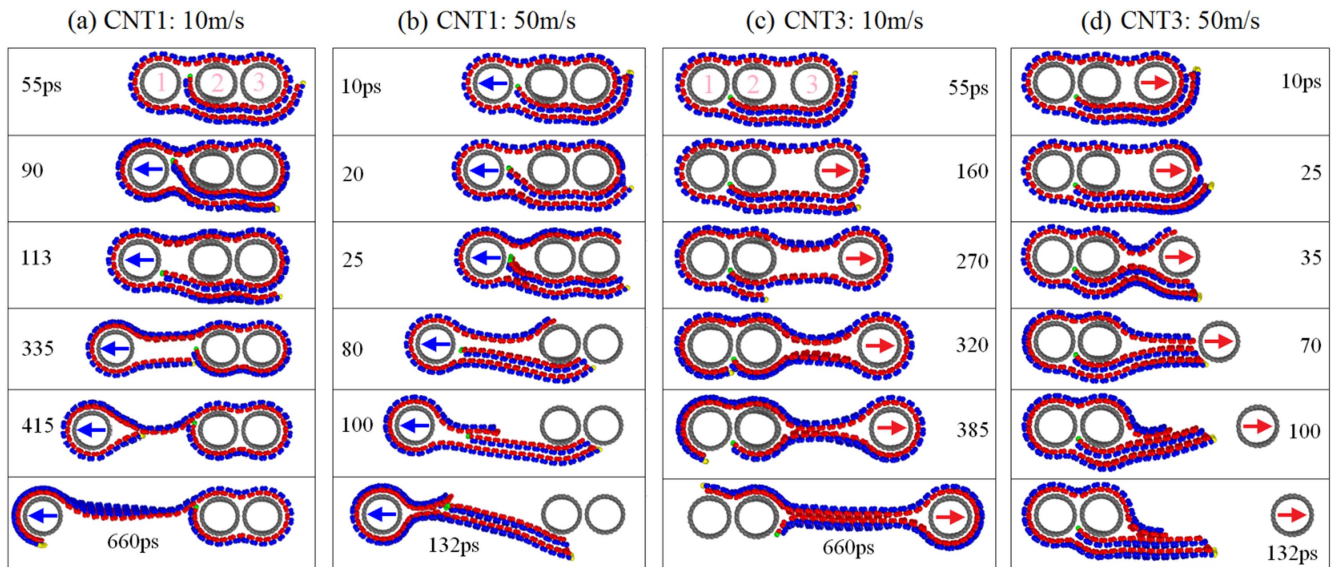


Figure 8. Snapshots of a 3-a-type system with a CNT moving in different motion schemes. (a) CNT1 moves to the left at 10 m s^{-1} ; (b) CNT1 moves to the left at 50 m s^{-1} ; (c) CNT3 moves to the left at 10 m s^{-1} ; (d) CNT3 moves to the left at 50 m s^{-1} .

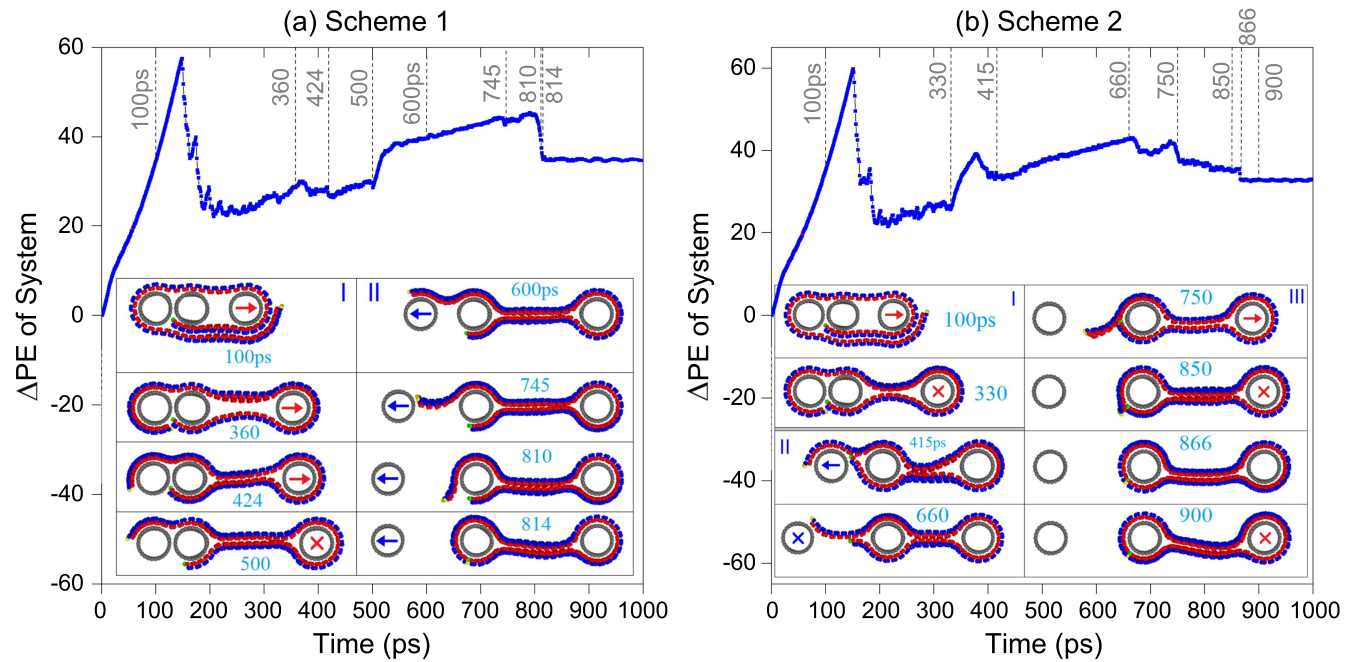


Figure 9. Histories of the potential energy variation of the 3-a-type system with a BP ribbon of $N = 55$, and two motion schemes of CNTs. (a) Results for scheme 1; (b) results for scheme 2.

both CNT2 and CNT3, move CNT1 to the left without stopping;

Scheme 2: (I) fix both CNT1 and CNT2, move CNT3 to the right for 3.3 nm, and stop; (II) fix both CNT2 and CNT3, move CNT1 to the left for 3.3 nm, and stop; (III) fix both CNT1 and CNT2, move CNT3 to the right for 1.5 nm, and stop.

In scheme 1, the displacement of CNT3 is chosen to be 5 nm according to the geometry of the system and equation (1). For example, if BP tends to be a ring wrapped around two CNTs, e.g., CNT2 and CNT3, the strong attraction between the upper and lower mid parts of BP should be

considered (the snapshot at 424 ps in figure 9(a)). Making use of the radii of the CNTs, their surface distance S_{23} (see figure 1(a)), and the equilibrium distance between BP and CNT ($\sim 0.34 \text{ nm}$ in table 2), we estimate that a BP with the length of 23.998 nm (see BP 4 with $N = 55$ in table 1) has high probability of forming an ideal ring when $S_{23} = \sim 5.3 \text{ nm}$ ($\sim 5.0 + 0.34$). Before using this scheme to form a ring, one should know accurately the length of the BP. That is a drawback of this approach. In figure 9(a), the ΔPE history of the system with the first motion scheme is shown together with some typical snapshots of the system. During the movement of CNT3, the lower end of the BP is always

attracted at the corner between CNT1 and CNT2. Due to the strong attraction of the corner, the rest of the BP slides on the CNTs. After 500 ps of motion of CNT3, the two ends of BP are separated by CNT1 and CNT2, and the mid parts of BP attach to each other. When CNT3 moves, at 810 ps, the attraction of CNT1 to the upper end of the BP ribbon is weaker than that of CNT2. Hence, the upper end of the BP ribbon is attracted and rapidly approaches the lower end of the BP ribbon. At 814 ps, an ideal ring is formed from the BP ribbon when the two ends are bonded together, as can be judged by the sharp drop in the ΔPE curve between 810 and 814 ps.

In scheme 2, the surface distance between two neighboring CNTs, i.e., S_{12} and S_{23} , is set at ~ 3.6 nm ($3.3 + 0.34$). Actually, the value is variable, because the purpose of moving CNT1 and CNT3 away is to reduce the overlap length of BP attracted onto CNT1. The third step, i.e., moving CNT3 further, needs accurate motion control of CNT3 during an *in situ* experiment, because a greater displacement of CNT3 will lead to larger gap between both ends of the BP ribbon and further result in failure to form a ring. Figure 9(b) gives the ΔPE history of the system with the second motion scheme. During the first 140 ps, the value of ΔPE increases continuously due to the overlap reduction of the BP itself and the decrease of interaction between CNT3 and CNT2. At 330 ps, the two ends of the BP are very close, unlike the previous position (figure 5(b)) where the two ends overlap rather bond together. By stopping CNT3 and moving CNT1 to the left for 3.3 nm, the upper end of the BP ribbon is still attracted onto CNT1 with small overlap. From our previous discussion (figure 3(a)) we know that the upper side of the BP ribbon, the configuration of the system at 750 ps is stable if all the CNTs are fixed. In this situation, we fix CNT1 and CNT2, and move CNT3. The overlap length of the mid parts of the BP ribbon increases with the decrease in the upper end part of the BP ribbon (movie 7). When the unsaturated phosphorus atoms at both ends of the BP ribbon are bonded together at 866 ps, the BP ring is finally formed.

4. Conclusions

To form an ideal ring from a rectangular BP ribbon on a CNT bundle, we investigate factors including length of the BP ribbon, layout type of the BP ribbon, and motion schemes for the CNTs that affect the formation of a nanoring. In numerical experiments in particular, in accordance with the perfect length of the BP ribbon, we choose three types of BP ribbon with lengths shorter than, longer than, and equal to the perfect length. In a 3-a-type model, an ideal ring can be formed from a ribbon with the length close to the perfect length. In summary, the following conclusions are drawn for potential applications:

- (1) a BP ribbon with the perfect length cannot form an ideal ring without moving any CNT away from the CNT bundle;
- (2) a BP ribbon with the perfect length can form a non-ideal ring in a 3-b-type model. If specifically an ideal ring is required, we must carefully create the initial layout of the BP ribbon;
- (3) there should be at least three CNTs in the bundle, among which a mid CNT is fixed to attract the two ends of the BP ribbon;
- (4) if an end of the BP ribbon becomes trapped at a corner between two neighboring fixed CNTs, it will not be possible for both ends to bond together;
- (5) when the mid CNT has been chosen, it is essential to move either the left or the right CNTs to reduce the distance between the two ends of the BP ribbon. Complex motion of the CNTs is preferable for forming a BP ring from the ribbon.

References

- [1] Qiao J, Kong X, Hu Z-X, Yang F and Ji W 2014 High-mobility transport anisotropy and linear dichroism in few-layer black phosphorus *Nat. Commun.* **5** 4475
- [2] Li L, Yu Y, Ye G J, Ge Q, Ou X, Wu H, Feng D, Chen X H and Zhang Y 2014 Black phosphorus field-effect transistors *Nat. Nanotechnol.* **9** 372–7
- [3] Fei R and Yang L 2014 Strain-engineering the anisotropic electrical conductance of few-layer black phosphorus *Nano Lett.* **14** 2884–9
- [4] Kroto H W, Heath J R, O'Brien S C, Curl R F and Smalley R E 1985 C-60—buckminsterfullerene *Nature* **318** 162–3
- [5] Qin Z, Qin Q H and Feng X Q 2008 Mechanical property of carbon nanotubes with intramolecular junctions: molecular dynamics simulations *Phys. Lett. A* **372** 6661–6
- [6] Qiu W, Kang Y L, Lei Z K, Qin Q H and Li Q 2009 A new theoretical model of a carbon nanotube strain sensor *Chin. Phys. Lett.* **26** 080701
- [7] Novoselov K S, Geim A K, Morozov S V, Jiang D, Zhang Y, Dubonos S V, Grigorieva I V and Firsov A A 2004 Electric field effect in atomically thin carbon films *Science* **306** 666–9
- [8] Sorokin A and Su H 2013 The mechanism of transforming diamond nanowires to carbon nanostructures *Nanotechnology* **25** 035601
- [9] Cai K, Wan J, Yu J, Cai H and Qin Q H 2016 Molecular dynamics study on welding a defected graphene by a moving fullerene *Appl. Surf. Sci.* **377** 213–20
- [10] Qiu W, Kang Y L, Lei Z K, Qin Q H and Li Q 2010 Experimental study of the Raman strain Rosette based on the carbon nanotube strain sensor *J. Raman Spectrosc.* **41** 1216–20
- [11] Zhang R, Ning Z, Zhang Y, Zheng Q, Chen Q, Xie H, Zhang Q, Qian W and Wei F 2013 Superlubricity in centimetres-long double-walled carbon nanotubes under ambient conditions *Nat. Nanotechnol.* **8** 912–6
- [12] Qiu W, Li Q, Lei Z K, Qin Q H and Deng W L 2013 The use of a carbon nanotube sensor for measuring strain by micro-Raman spectroscopy *Carbon* **53** 161–8
- [13] Jiang J-W and Park H S 2014 Mechanical properties of single-layer black phosphorus *J. Phys. D: Appl. Phys.* **47** 385304
- [14] Sha Z-D, Pei Q-X, Ding Z, Jiang J-W and Zhang Y-W 2015 Mechanical properties and fracture behavior of single-layer phosphorene at finite temperatures *J. Phys. D: Appl. Phys.* **48** 395303

- [15] Island J O, Steele G A, van der Zant H S and Castellanos-Gomez A 2015 Environmental instability of few-layer black phosphorus *2D Mater.* **2** 011002
- [16] Doganov R A, O'Farrell E C, Koenig S P, Yeo Y, Ziletti A, Carvalho A, Campbell D K, Coker D F, Watanabe K and Taniguchi T 2015 Transport properties of pristine few-layer black phosphorus by van der Waals passivation in an inert atmosphere *Nat. Commun.* **6** 6647
- [17] Kang J, Wood J D, Wells S A, Lee J-H, Liu X, Chen K-S and Hersam M C 2015 Solvent exfoliation of electronic-grade, two-dimensional black phosphorus *ACS Nano* **9** 3596–604
- [18] Favron A, Gaufrès E, Fossard F, Phaneuf-L'Heureux A-L, Tang N Y, Lévesque P L, Loiseau A, Leonelli R, Francoeur S and Martel R 2015 Photooxidation and quantum confinement effects in exfoliated black phosphorus *Nat. Mater.* **14** 826–32
- [19] Huang Y, Qiao J, He K, Bliznakov S, Sutter E, Chen X, Luo D, Meng F, Su D and Decker J 2016 Interaction of black phosphorus with oxygen and water *Chem. Mater.* **28** 8330–9
- [20] Kim J, Baek S K, Kim K S, Chang Y J and Choi E 2016 Long-term stability study of graphene-passivated black phosphorus under air exposure *Curr. Appl. Phys.* **16** 165–9
- [21] Wood J D, Wells S A, Jariwala D, Chen K-S, Cho E, Sangwan V K, Liu X, Lauhon L J, Marks T J and Hersam M C 2014 Effective passivation of exfoliated black phosphorus transistors against ambient degradation *Nano Lett.* **14** 6964–70
- [22] Chen X, Wu Y, Wu Z, Han Y, Xu S, Wang L, Ye W, Han T, He Y and Cai Y 2015 High-quality sandwiched black phosphorus heterostructure and its quantum oscillations *Nat. Commun.* **6** 7315
- [23] Guo H, Lu N, Dai J, Wu X and Zeng X C 2014 Phosphorene nanoribbons, phosphorus nanotubes, and van der Waals multilayers *J. Phys. Chem. C* **118** 14051–9
- [24] Cai K, Wan J, Wei N, Cai H and Qin Q H 2016 Thermal stability of a free nanotube from single-layer black phosphorus *Nanotechnology* **27** 235703
- [25] Cai K, Wan J, Wei N and Qin Q H 2016 Strength and stability analysis of a single-walled black phosphorus tube under axial compression *Nanotechnology* **27** 275701
- [26] Cai K, Liu L, Shi J and Qin Q H 2017 Winding a nanotube from black phosphorus nanoribbon onto a CNT at low temperature: a molecular dynamics study *Mater. Des.* **121** 406–13
- [27] Safae S M R, PilAli A and Karami M A 2017 Nanoscale plasmonically enhanced photodetector based on a gold nanoring *Appl. Opt.* **56** 476–81
- [28] Xing R and Jian S S 2016 Numerical analysis on the multilayer nanoring waveguide pair *IEEE Photon. Technol. Lett.* **28** 2779–82
- [29] Kouno T, Takeshima H, Kishino K, Sakai M and Hara K 2016 Biosensors based on GaN nanoring optical cavities *Japan. J. Appl. Phys.* **55** 05FF05
- [30] Parkinson P, Kamonsutthipajit N, Anderson H L and Herz L M 2016 Size-independent energy transfer in biomimetic nanoring complexes *ACS Nano* **10** 5933–40
- [31] Lee S H, Choi S M, Yoon S, Jeong H, Jung G Y, Cho B K and Kim W B 2014 Transfer printing of metal nanoring and nanodot arrays for use in catalytic reactions *Chem. Commun.* **50** 8472–5
- [32] Lu D P, Wu H T, Dai Y F, Shi H, Shao X, Yang S F, Yang J L and Du P W 2016 A cycloparaphenylene nanoring with graphenic hexabenzocoronene sidewalls *Chem. Commun.* **52** 7164–7
- [33] Halpern A R and Corn R M 2013 Lithographically patterned electrodeposition of gold, silver, and nickel nanoring arrays with widely tunable near-infrared plasmonic resonances *ACS Nano* **7** 1755–62
- [34] Hobbs K L, Larson P R, Lian G D, Keay J C and Johnson M B 2004 Fabrication of nanoring arrays by sputter redeposition using porous alumina templates *Nano Lett.* **4** 167–71
- [35] Cui B and Veres T 2007 Fabrication of metal nanoring array by nanoimprint lithography (NIL) and reactive ion etching *Microelectron. Eng.* **84** 1544–7
- [36] Chien H H and Wu H C 2012 Fabrication of size-tunable hierarchical porous Cr nanoring arrays by modified nanosphere lithography *Micro Nano Lett.* **7** 1033–7
- [37] Cai K, Liu L, Shi J and Qin Q H 2017 Self-assembly of a jammed black phosphorus nanoribbon on a fixed carbon nanotube *J. Phys. Chem. C* **121** 10174–81
- [38] Cai K, Wan J, Wei N, Shi J and Qin Q H 2017 Buckling behaviour of composites with double wall nanotubes from carbon and phosphorous *Phys. Chem. Chem. Phys.* **19** 10922–30
- [39] Shi J, Cai H, Cai K and Qin Q H 2017 Dynamic behavior of a black phosphorus and carbon nanotube composite system *J. Phys. D: Appl. Phys.* **50** 025304
- [40] Appalakondaiah S, Vaitheeswaran G, Lebegue S, Christensen N E and Svane A 2012 Effect of van der Waals interactions on the structural and elastic properties of black phosphorus *Phys. Rev. B* **86** 035105
- [41] Plimpton S 1995 Fast parallel algorithms for short-range molecular dynamics *J. Comput. Phys.* **117** 1–19
- [42] Stuart S J, Tutein A B and Harrison J A 2000 A reactive potential for hydrocarbons with intermolecular interactions *J. Chem. Phys.* **112** 6472–86
- [43] Stillinger F H and Weber T A 1985 Computer simulation of local order in condensed phases of silicon *Phys. Rev. B* **31** 5262
- [44] Jiang J-W 2015 Parametrization of Stillinger–Weber potential based on valence force field model: application to single-layer MoS₂ and black phosphorus *Nanotechnology* **26** 315706
- [45] Jones J E 1924 On the determination of molecular fields. II. From the equation of state of a gas *Proc. R. Soc. A* **106** 463–77
- [46] Sorkin V and Zhang Y 2015 The structure and elastic properties of phosphorene edges *Nanotechnology* **26** 235707